

Impact of Lake Breezes on Summer Ozone Concentrations in the Salt Lake Valley

BRIAN K. BLAYLOCK, JOHN D. HOREL, AND ERIK T. CROSMAN

Department of Atmospheric Sciences, University of Utah, Salt Lake City, Utah

(Manuscript received 10 June 2016, in final form 19 September 2016)

ABSTRACT

During the late afternoon of 18 June 2015, ozone concentrations in advance of a strong lake-breeze front arising from the Great Salt Lake in northern Utah were ~20 ppb lower than those in its wake. The lake-breeze progression and ozone concentrations in the valley were monitored by an enhanced observation network that included automated weather stations, a nearby Terminal Doppler Weather Radar, state air quality measurement sites, and mobile platforms, including a news helicopter. Southerly flow opposing the lake breeze increased convergent frontogenesis and delayed the onset of its passage through the Salt Lake valley. Ozone concentrations were exceptionally high aloft at the lake-breeze frontal boundary. The progression of this lake breeze was simulated using the Weather Research and Forecasting Model at 1-km horizontal grid spacing over northern Utah. The model was initialized using hourly analyses from the High Resolution Rapid Refresh model. Errors in the underlying surface initialization were improved by adjusting the areal extent and surface temperature of the lake to observed lake conditions. An urban canopy parameterization is also included. The opposing southerly flow was weaker in the simulation than that observed such that the simulated lake-breeze front occurred too early. Continuous passive tracers initialized within and ahead of the lake breeze highlight the dispersion and transport of pollutants arising from the lake-breeze front. Tracers within the lake breeze are confined near the surface while tracers in advance of the front are lofted over it.

1. Introduction

Tropospheric ozone is harmful to human health with the greatest impact on children, the elderly, and individuals with respiratory diseases (Sousa et al. 2013). The Environmental Protection Agency (EPA) tightened the National Ambient Air Quality Standard (NAAQS) for ozone from 75 to 70 ppb (EPA 2015). Metropolitan and rural areas in the western United States may have difficulty complying with this standard since background ozone levels are often high in this region (Jaffe 2011). Thus, implementing effective ozone reduction plans and improving air quality forecasts in these states requires a deeper understanding of local factors that exacerbate ozone pollution.

Air quality in the highly urbanized corridor on the east side of the Great Salt Lake (GSL) in northern Utah is largely controlled by its complex geography (Fig. 1a) and attendant meteorology. The densely populated Salt Lake valley to the southeast of the GSL is bounded by the Wasatch Mountains to the east and the Oquirrh

Mountains to the west (Fig. 1b). The surrounding terrain, variable underlying land surface characteristics, and the GSL contribute to thermally driven flows that influence the development, transport, and destruction of air pollutants within the valley (Stewart et al. 2002; Ludwig et al. 2004). For example, afternoon lake breezes penetrating southward into the Salt Lake valley are common on clear summer days and arise from differential heating between the GSL, the valley floor, and the surrounding terrain (Zumpfe and Horel 2007). These lake breezes are typically superimposed on the daytime upvalley flow, which provides a continuous daytime upvalley transport mechanism throughout the Salt Lake valley on synoptically undisturbed days (Crosman and Horel 2010).

Anthropogenic emissions and photochemical reactions are directly responsible for the production of ozone (Monks et al. 2015). Variations in the horizontal and vertical transport of ozone and its chemical precursors modulate ozone concentrations observed at specific locales and times. For example, Lennartson and Schwartz (2002) and Wentworth et al. (2015) found that elevated ozone levels are more frequently observed during afternoons when lake breezes are present. Pollutant transport

Corresponding author e-mail: Brian Blaylock, brian.blaylock@utah.edu

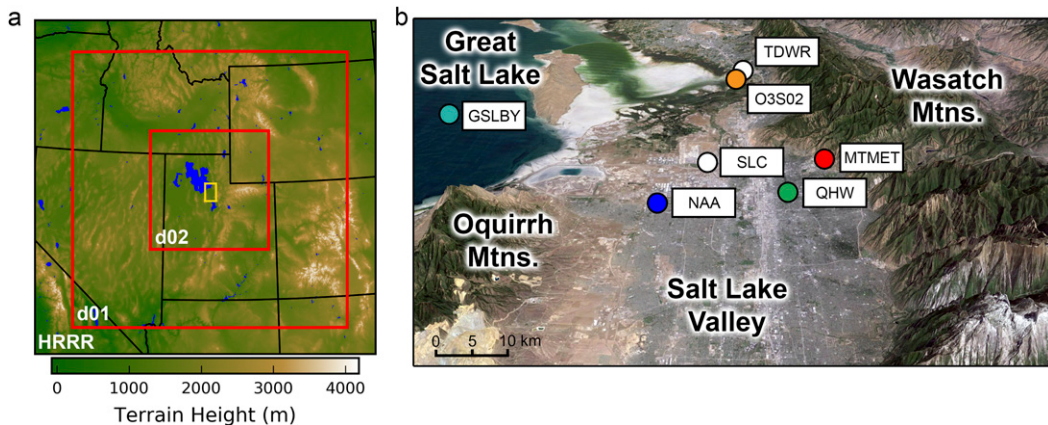


FIG. 1. (a) HRRR model terrain (shaded according to scale) with nested WRF domains outlined in red and the Salt Lake valley region outlined in yellow. (b) Observation sites discussed in the text: GSLBY, TDWR, SLC, O3S02, NAA, MTMET, and QHW.

by sea and lake breezes has been extensively studied in many coastal metropolitan areas, for example, Los Angeles, California (Lu and Turco 1995); Milwaukee, Wisconsin (Lennartson and Schwartz 2002); Houston, Texas (Banta et al. 2005); Chicago, Illinois (Foley et al. 2011); Maryland (Stauffer et al. 2015); Toronto, Ontario, Canada (Hastie et al. 1999; Wentworth et al. 2015); and southwest Ontario (Levy et al. 2010; Hayden et al. 2011; Sills et al. 2011). From these and other studies, it is recognized that vertical mixing, horizontal advection, and recirculation within thermally driven coastal circulations strongly influence pollutant concentrations.

While nocturnal ozone depletion, through the combined effects of dry deposition and titration by nitrous oxides, is often observed in urban regions (Talbot et al. 2005), dry deposition rates are lower over water surfaces (Monks et al. 2015). For instance, Goldberg et al. (2014) found that decreased deposition rates over the Chesapeake Bay likely contributed to higher ozone concentrations over the bay than the surrounding land surfaces. Similar results were also found over Lake Tahoe (Burley et al. 2015). When the sea- or lake-breeze circulation transports urban pollutants over the water at night, the reduced deposition rates preserve the transported pollutants for subsequent advection back inland the following day. This recirculation of pollutants combined with the limited vertical mixing within the shallow boundary layer of the lake breeze can elevate urban ozone concentration as the lake or sea breeze advects inland (Foley et al. 2011; Wentworth et al. 2015).

The interactions between the large-scale synoptic environment and thermally driven circulations also modulate the day-to-day variability in pollutant concentrations in coastal regions. When the prevailing flow opposes the afternoon breeze, convergent frontogenesis

at its leading edge is common, which can lead to a delayed onset of the breeze circulation at the coastline, slower rates of inland frontal movement, and enhanced convergence within and behind the frontal zone (Arritt 1989; Arritt 1993; Gilliam et al. 2004; Porson et al. 2007; Crosman and Horel 2010; Ji et al. 2013). Several studies have documented the enhancement of pollutant concentrations resulting from convergent frontogenesis of sea- and lake-breeze fronts. Gaza (1998) found elevated ozone and precursors in a narrow zone along and behind a sea-breeze coastal boundary in the northeastern United States associated with convergence and a strong capping inversion behind the front. Oh et al. (2006) and Hwang et al. (2007) found enhanced ozone concentrations due to convergent frontogenesis and a stalled sea-breeze front during opposing flow in the nearshore regions of several metropolitan areas in Korea. In the Salt Lake valley, convergent frontogenesis along a wintertime lake-breeze front was shown to impact PM_{2.5} concentrations in the Salt Lake valley (Crosman and Horel 2016).

High ozone concentrations during summer involving sea or lake breezes have been difficult to simulate and forecast, especially in operational numerical air quality models (Lu and Turco 1995; Banta et al. 2005; Angevine et al. 2006; Bao et al. 2008; Crosman and Horel 2010; Angevine et al. 2012). Inaccurate initializations, including incomplete specification of coastline characteristics and water surface temperatures, are some of the factors impeding such numerical forecasts (Crosman and Horel 2012; Lombardo et al. 2016).

As described by Horel et al. (2016), Utah's Division of Air Quality (DAQ) initiated the Great Salt Lake Summer Ozone Study (GSLSO₃S) in 2015 to develop a more complete understanding of the GSL's influence on summer

ozone. The specific objectives of GSLSO₃S were to 1) determine the areal and vertical extent of summer ozone over and surrounding the GSL and 2) enhance our understanding of the physical processes that control summer ozone near the GSL to improve air quality forecasts for the urban regions adjacent to the GSL. The work presented here represents the first detailed study designed to investigate how lake breezes affect ozone concentrations near the GSL.

We focus here on lake breezes affecting ozone pollutant concentrations on 17–18 June 2015. Over the six days prior to 17 June, none of the 18 ozone observation locations in the vicinity of the GSL or nearby urban areas observed 8-h averaged ozone concentrations in excess of 70 ppb, whereas on 17 and 18 June NAAQS exceedances were observed at 7 and 12 sites, respectively. The following day, 19 June, no stations exceeded the threshold.

The case studies by [Zumpfe and Horel \(2007\)](#) and [Crosman and Horel \(2016\)](#) illustrate how GSL breezes occurring during all seasons can vary in terms of onset time, propagation speed, and frontal intensity. We view the lake breeze on 17 June as a canonical case with features common to many others examined over the years. We will draw greater attention to the lake breeze on 18 June because of its later onset and stronger intensity resulting from enhanced convergent frontogenesis of the lake breeze. In addition, the role of the lake breeze on ozone concentrations reverses between the two day—the lake serves as a reservoir of cleaner air on 17 June but has more polluted air on 18 June. A high-resolution numerical simulation of the lake breezes on those two days is evaluated relative to the available observations. Passive tracers available from the simulation illustrate how pollutants within the lake breeze on 18 June may have been concentrated within the shallow boundary layer of the lake breeze.

2. Data and method

a. GSLSO₃S observations

[Horel et al. \(2016\)](#) summarize that the GSLSO₃S took advantage of existing observational infrastructure as well as deployed additional sensors during the summer study. Atmospheric conditions in northern Utah were monitored at over a hundred in situ automated surface stations available through the MesoWest cooperative network ([Horel et al. 2002](#)). Near-surface and upper-air observations near the lake are available from rawinsondes launched at the Salt Lake International Airport (SLC in [Fig. 1b](#)) during the morning (1200 UTC) and evening (0000 UTC). A Terminal Doppler Weather

Radar (TDWR) located directly north of the Salt Lake valley (see [Fig. 1b](#)) measured radial wind velocities in the western half of the Salt Lake valley (beam blockage by intervening terrain restricts observation in the eastern half of the valley). A buoy in the south arm of the GSL (GSLBY) deployed by the U.S. Geological Survey (USGS) measured meteorological parameters and water temperature at 14 levels in the vertical. Ozone concentrations in northern Utah were measured at eight permanent DAQ sites with 16 temporary sensors deployed by DAQ and the University of Utah, each with federal equivalent method (FEM) ozone monitors that were calibrated at the outset of the study ([Horel et al. 2016](#)). We focus here on four sites with ozone sensors collocated with meteorological sensors—Farmington Bay (O3S02), Neil Armstrong Academy in West Valley (NAA), the DAQ's Hawthorne site (QHW), and the University of Utah's Mountain Meteorology Laboratory (MTMET) ([Fig. 1b](#)). The sampling interval at O3S02, NAA, and MTMET was 5 min whereas QHW had a sampling interval of 15 min.

Additional calibrated FEM ozone sensors were mounted in enclosed spaces with short inlet tubes (0.5–1.5-m length) extending outward from them on 1) a public-transit light rail car, known as TRAX, operating on electrified routes in the Salt Lake valley, and 2) the KSL-TV news helicopter. The reporting intervals for these ozone observations were 1 min and 10 s, respectively. Many of the helicopter's summer flight times and flight paths were determined by the pilot's routine traffic reports and other news reporting needs. We requested the pilot make an overflight of the GSL during the afternoon of 17 June 2015 with vertical profiles from close to the surface to 1000 m AGL. Fortunately, during the afternoon of 18 June 2015, the pilot flew the helicopter down the center of the valley through the lake-breeze front at elevations between 1400 and 1700 m MSL (100–400 m AGL).

b. WRF model

1) MODEL CONFIGURATION

A high-resolution simulation of the atmospheric conditions for the lake breezes on 17–18 June 2015 was completed using version 3.7 of the Weather Research and Forecasting (WRF) Model with the Advanced Research WRF dynamical core (see [Table 1](#) for a summary of the configuration details). Initial and boundary conditions were retrieved from the National Centers for Environmental Prediction High Resolution Rapid Refresh (HRRR) model hourly analyses beginning at 0000 UTC 14 June 2015 and continuing until 0700 UTC 19 June 2015 ([Benjamin et al. 2016](#)). Two WRF domains

TABLE 1. WRF model configuration.

Setting or option	Domain d01 (d02)
WRF version	WRF 3.7
Boundary conditions	HRRR (d01)
Land surface	30 arc-s MODIS 21 category
dx/dy	3 km (1 km)
No. of vertical levels	30
Model top	50 hPa
Microphysics	Thompson
Radiation	RRTMG
Planetary boundary layer	Mellor–Yamada–Janjić
Surface layer	Unified Noah land surface model
Cumulus scheme	No cumulus parameterization

with one-way nesting within the 3-km horizontal resolution HRRR domain were used, as shown in Fig. 1a. The outer 3-km domain, d01, covers all of Utah and parts of the surrounding states while the inner 1-km domain, d02, is focused on northern Utah. Both domains are centered over Salt Lake City with 30 vertical eta levels between the surface and 50 hPa. The MODIS 30-arc-s land-use classification—also used by the HRRR model—is used here except for the modifications discussed in the next subsection.

2) WRF MODIFICATIONS

Lombardo et al. (2016) discuss the sensitivity of simulated sea breezes in Connecticut and New York to inaccurate coastlines and sea surface temperatures when initializing simulations from coarse 32-km North America Regional Reanalysis grids. These types of errors are evident in the 3-km HRRR near the GSL as well. Inspection of the land-use categories within the HRRR model revealed errors in the areal extent of the GSL arising from the reliance on a 2001 MODIS image when the lake level was much higher than in 2015 (Fig. 2b). The GSL lies within an endorheic basin whose level has been strongly affected by drought and increased water use (Wurtsbaugh et al. 2016). During the 2015 summer, the GSL was near record low levels, as evident in the MODIS image for 18 June 2015 (Fig. 2a). The specified lake temperature in the HRRR analyses was also much too low (Table 2).

To overcome the deficiencies in the areal extent and lake temperature available from the HRRR, Fig. 2c illustrates the modifications applied for the WRF simulations. Model grid points that are no longer lake were reclassified as “barren or sparsely vegetated” land to represent the exposed, dry lake bed (cf. Figs. 2b and 2c). In addition to the average HRRR lake temperature being too cold (Table 2), the lowest temperatures are skewed toward the southwest of the lake’s boundary and the lake-edge temperatures are affected by land

temperature contamination (Fig. 2b inset). Based on lake temperature climatology (Crosman and Horel 2009), along with available estimates of lake surface temperature from an AVHRR thermal image at 2330 UTC 18 June 2015 and subsurface temperature from the GSLBY buoy on that day, the temperature of the GSL was modified to a uniform temperature of 28.9°C (302 K) to represent the afternoon lake surface temperature (see Fig. 2c inset). Although land surface temperatures evolve on the basis of the Noah land surface model parameterization, the lake surface temperature remains fixed throughout the simulation.

The treatment of urban effects in the Salt Lake valley was also improved by enabling the urban canopy model for the WRF Model, which is not used in the HRRR. Parameters in that scheme were modified to better represent the Salt Lake valley. For example, the Salt Lake valley during summer contains many regions that resemble an urban forest with dense vegetation and large swaths of irrigated lawns. Thus, the percentage of vegetation in the urban land-use category was increased from the default setting of 10%–50% to help reduce near-surface wind speeds and cool the urban area. Small increases in the average building height and road width were also made from the default settings to conform more closely to the local environment.

3. Results and discussion

a. 17–18 June lake-breeze events

The synoptic weather pattern during the week encompassing 17–18 June 2015 was dominated by a long-wave ridge of high pressure over the western United States. These conditions led to low cloud amounts and strong solar insolation—an optimal environment for both a strong lake breeze and photochemical production of ozone. On 17 June, the background synoptic flow remained weak and the lake-breeze system developed largely uninfluenced by the synoptic flow. These situations are often referred to as “classic” lake-breeze cases in the literature (Crosman and Horel 2010). On 18 June, however, channeled synoptic flow led to enhanced southerly flow into the Salt Lake valley, resulting in the ideal conditions for convergent frontogenesis of the lake-breeze front.

Potential temperature, mixing ratio, and wind profiles below 3800 m MSL at SLC are shown for the morning and evening of 18 June in Fig. 3. In the morning sounding, a radiational inversion below 2000 m MSL is evident with southeasterly winds caused by the down-valley land breeze toward the GSL (Fig. 3a). Focusing on the observations above 1500 m MSL, since the surface

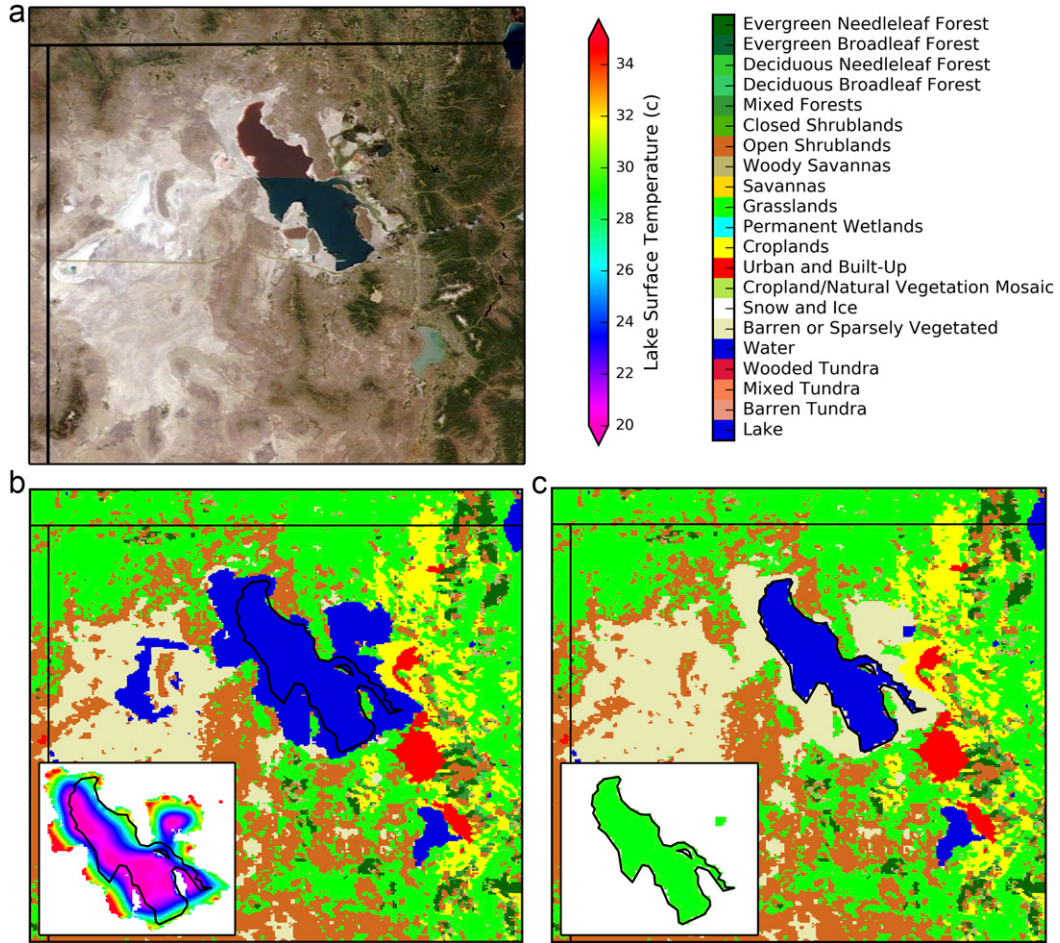


FIG. 2. (a) MODIS true-color satellite image from 18 Jun 2015. (b) MODIS 30-arc-s land-use categories (defined by the color bar at the top right) used in HRRR and the WRF Model with Great Salt Lake at record high levels and a pool of water in the west desert. The black outline delineates the lake extent during summer 2015. The inset shows the Great Salt Lake's size and lake surface temperature (according to the color bar at the top right) initialized by HRRR analyses. (c) As in (b), but for the lake size adjusted to 2015 level. Inset shows the modified lake size with uniform lake surface temperature (28.9°C).

values at the SLC airport are likely not representative of the larger valley environment, the neutral lapse rate in the evening sounding reflects strong mixing leading to nearly constant mixing ratios (Fig. 3b). Northwest winds below 2000 m MSL and the slightly higher mixing ratio value at \sim 1600 m MSL are the signatures of the intrusion of the lake breeze past the airport accompanied by opposing winds aloft of $5\text{--}10 \text{ m s}^{-1}$ from the south-southwest above 3000 m MSL.

The lake breezes progressing through the Salt Lake valley during the afternoons of 17 and 18 June were observed continuously by the TDWR and in situ weather stations. These observations highlight the differences in the lake-breeze propagation between the two days. Snapshots of their progression are provided in Fig. 4. Downvalley winds toward the GSL dominate the western

two-thirds of the Salt Lake valley during both mornings, as evident in Figs. 4a and 4d (1800 UTC is an hour before solar noon). The southerly downvalley flow on 18 June is enhanced by channeled synoptic flow through the gaps of the Traverse Range at the southern extent of the Salt Lake valley (Lareau and Horel 2015). The stronger southerly winds on 18 June extended over 6 km farther

TABLE 2. Estimates of Great Salt Lake temperature for 18 Jun 2015.

	Lake temperature (°C)
Afternoon buoy water temperature at 0.4 m below surface	27.3
AVHRR satellite [2330 UTC (1730 LT)]	27–30
HRRR lake-area average	22.5
WRF modified (see Fig. 2c)	28.9

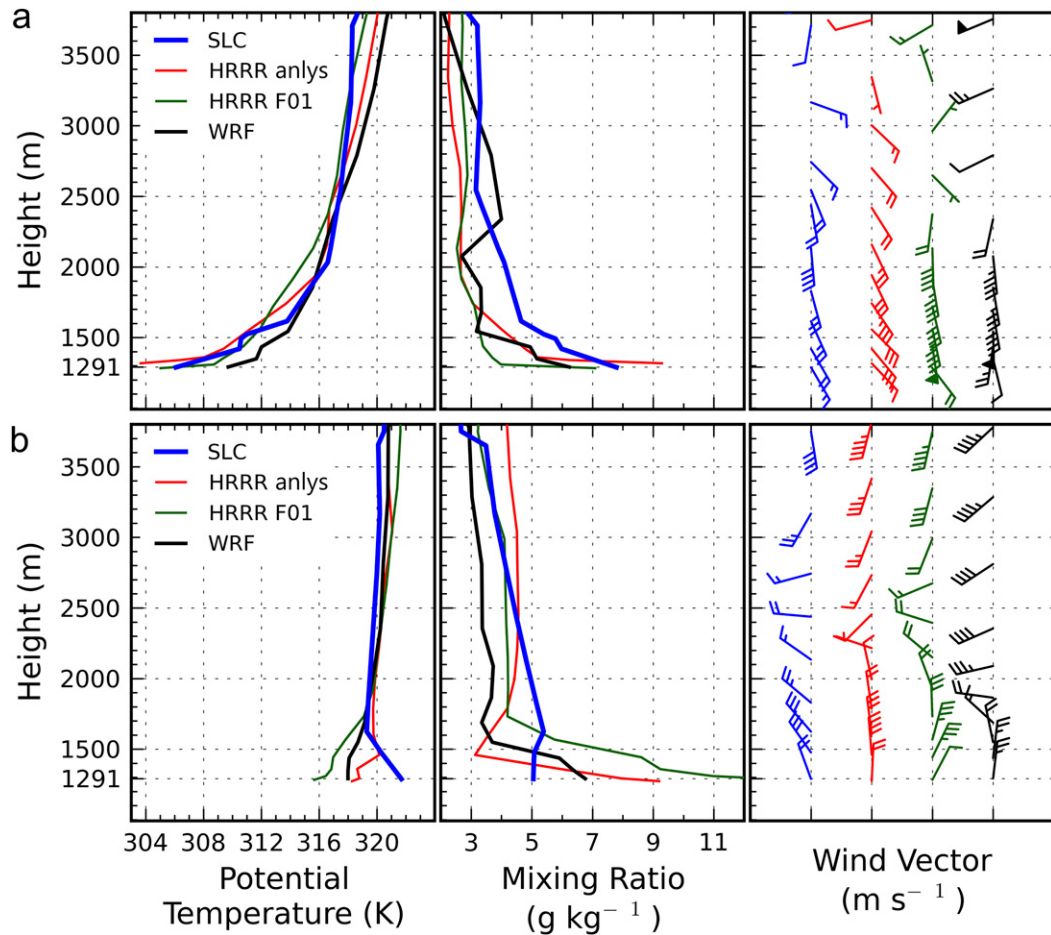


FIG. 3. Vertical profiles of potential temperature, mixing ratio, and vector winds at SLC from the SLC rawinsonde (blue), HRRR analysis (red), HRRR 1-h forecast (green), and WRF simulation (black) at (a) 1200 UTC 18 Jun 2015 and (b) 0000 UTC 19 Jun 2015. Half and full wind barbs and flags denote 1, 2, and 10 m s^{-1} , respectively.

north (past SLC; white circle in Fig. 4) than what was observed the previous day. Northwest winds in the northwest corner of the valley closest to the GSL opposed the downvalley flows during the mornings. Common to many lake-breeze events (Crosman and Horel 2016), the lake-breeze boundary on 17 June traversed southward through much of the valley by 2100 UTC with distinct pulses during that afternoon (i.e., inbound–outbound radial velocity couplets are evident in the western half of the valley). By 0000 UTC 18 June (Fig. 4c), the lake breeze has transited through the entire valley. On the following day, however, the boundary between the downvalley and lake-breeze flows and associated convergent frontogenesis remained quasi-stationary because of the stronger southerly winds until after 2000 UTC on 18 June. Temperature, moisture, and ozone concentration discontinuities began to strengthen across that boundary. By 2100 UTC 18 June, the wind shift boundary began to move southward in the center of the valley,

passing over SLC, and exhibiting the characteristics of a well-defined lake-breeze front (Fig. 4e). The front progressed down the valley at a relatively slow phase speed of $4\text{--}6 \text{ km h}^{-1}$ (Fig. 4f) until reaching the southern terminus of the valley by 0200 UTC 19 June (not shown). During both evenings, the lake breezes rapidly collapsed and southerly winds returned to the valley surface.

The time series in Fig. 5 of observed temperature, vector wind, and ozone concentrations highlight similarities and differences between the lake breezes during these two afternoons. Consider first the underlying driver of the land and lake breezes evident from the differences in air temperature between the buoy (GSLBY) relative to the other sites—higher temperatures over the lake during early morning and lower temperatures during the afternoon. The temperatures and ozone concentrations at O3S02, north of the SLC airport, increased during both mornings, with peak ozone values of 85–90 ppb near solar noon (1900 UTC). The midday ozone concentrations at

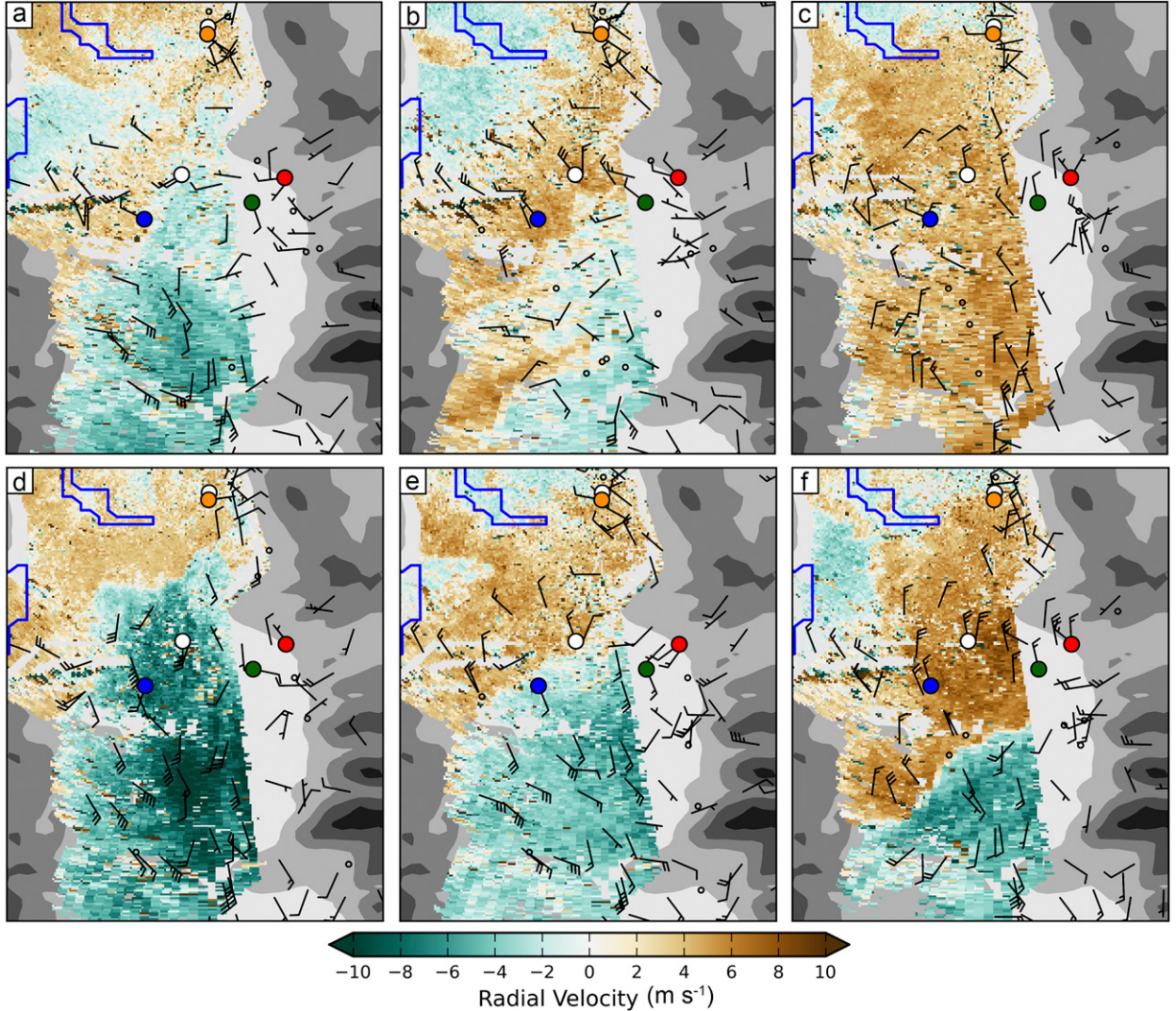


FIG. 4. TDWR 0.5° radial velocity and MesoWest surface wind observations at (a) 1800 UTC 17 Jun 2015, (b) 2100 UTC 17 Jun 2015, (c) 0000 UTC 18 Jun 2015, (d) 1800 UTC 18 Jun 2015, (e) 2100 UTC 18 Jun 2015, and (f) 0000 UTC 19 Jun 2015. Terrain is indicated by successively darker gray shades at 500-m intervals with the approximate shoreline of the Great Salt Lake outlined in blue. Color shading indicates radial velocity with respect to the TDWR located at the top of the map according to the color bar. Vector winds at observation sites are marked by wind bars where half and full bars denote 1 and 2 m s^{-1} , respectively. Colored dots denote observation sites highlighted in Fig. 1b.

this station are likely influenced by several factors: 1) transported precursor pollutants from urban areas to its east and south, 2) permanent wetlands to the south potentially providing biogenic precursor chemicals, and 3) a highly reflective playa to the north enhancing photochemical production. The influence of the GSL's main water body to the west is evident by the lake-breeze push from that direction at 2100 UTC 17 June and 2000 UTC 18 June followed by reduced ozone concentrations. The ozone concentrations at O3S02 decreased below 70 ppb on 17 June and hovered around 80 ppb on 18 June after the passages of the lake breezes; that is, the ozone

concentrations arriving from the direction of the main body of the GSL were lower than the peak value observed at O3S02 at solar noon each day.

Differences in the transition from down- to upvalley flows are evident during the two days at NAA located in the western sector of the valley (Fig. 5c). Two early pulses of northerly–northwesterly winds are evident at 1700 and 1900 UTC 17 June followed by the more sustained northwesterly push after 2000 UTC that is coupled with a sharp drop in temperature, both of which indicate the lake-breeze front transiting NAA (refer as well to Fig. 4b). Ozone concentrations remain at

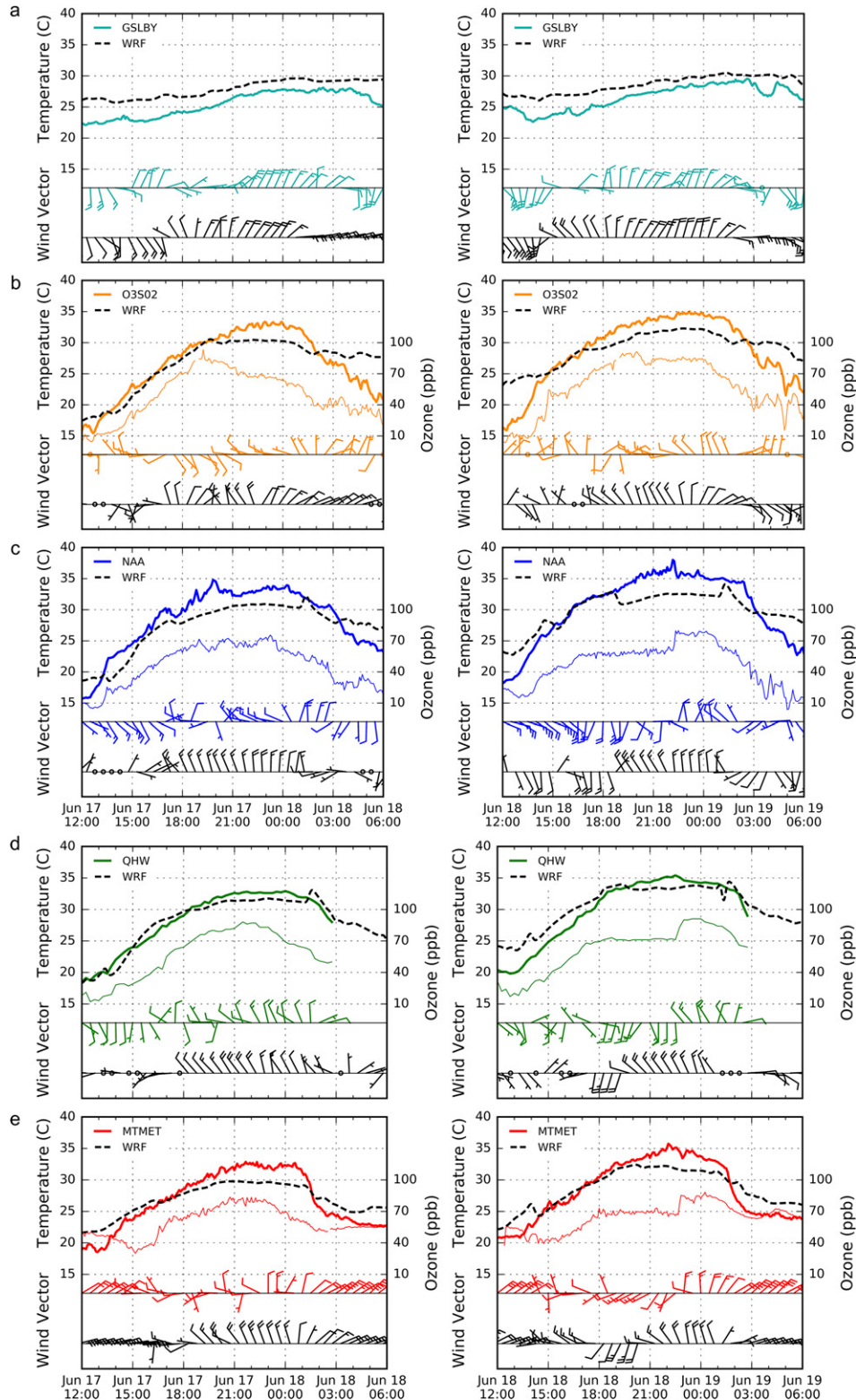


FIG. 5. Observed (thick color) and simulated (dashed black) temperature, observed ozone (thin color) and vector wind (left) between 1200 UTC 17 Jun and 0600 UTC 18 Jun 2015 and (right) between 1200 UTC 18 Jun and 0600 UTC 19 Jun 2015. Wind barbs are plotted every half hour with half and full barbs denoting 1 and 2 m s⁻¹, respectively.

~70 ppb throughout the rest of the afternoon. During the late morning on 18 June, stronger southerly flow opposed the lake breeze and ozone concentrations of ~60 ppb persisted until 2200 UTC, at which point there is a sharp decrease in temperature and sharp increase in ozone levels. Observations from a sonic detection and ranging (sodar) device located 4.5 km to the north of NAA also documented the early (1700 UTC) switch from downvalley to weak westerly–northwesterly winds on 17 June. However, on 18 June between 1700 and 1900 UTC the downvalley winds below 100 m observed by the sodar persisted and actually increased in speed to 8 m s^{-1} until the abrupt passage of the lake-breeze front (not shown).

Variable wind directions are observed before 2100 UTC on 17 June in the eastern urban corridor of the valley (e.g., QHW). Ozone concentrations rise steadily during the day, peaking near the same time as the final lake-breeze pulse, followed by a steady decrease in ozone ([Fig. 5d](#)). In contrast, sustained southerly flow during midday on 18 June contributes to nearly constant ozone concentrations until the arrival of the lake-breeze front, when a sharp ~20-ppb increase in ozone is observed, similar to that shown previously at NAA. On the easternmost fringe of the valley (MTMET), midmorning transitions between 1500 and 1800 UTC from easterly downslope/downcanyon flows to upslope westerly flows on both days led to sharp increases in ozone concentrations, presumably as a result of the local westerly transport of ozone and other pollutants from the nearby urban core. As the lake-breeze front transits NAA, QHW, and MTMET, ozone concentrations increased 15–20 ppb and remained elevated for several hours, which is consistent with the ozone levels observed at O3S02 after the lake-breeze passage. After 0000 UTC 19 June and throughout the evening, ozone is reduced at O3S02, NAA, and QHW while concentrations remain elevated (>60 ppb) at MTMET, which is consistent with higher background ozone concentrations observed during the evening from an FEM ozone monitor in the Wasatch Mountains (not shown).

The KSL-TV helicopter transect from 2050 to 2200 UTC 17 June was the most extensive flight over the GSL during the summer ([Fig. 6a](#)). The helicopter transited clockwise, originating from near O3S02, and completed two spiral profiles over the GSL, with the southernmost spiral over GSLBY. Ozone concentrations over the GSL at the predominant flight level of 1550 m MSL (250 m AGL) ranged between 50 and 60 ppb. When the helicopter descended lower than 1350 m MSL (50 m AGL), ozone concentrations increased to 60 ppb in the first spiral and 70 ppb in the second spiral. When ascending above 2300 m MSL (1000 m AGL), ozone then dropped below

50 ppb. Hence, the air with the highest ozone concentrations over the lake was confined within a thin layer over the GSL that afternoon while the urban area east of the lake observed higher ozone concentrations between 65 and 87 ppb ([Fig. 6a](#)).

An afternoon KSL-TV helicopter transect on 18 June was a more typical flight during the summer, transiting from south to north through the Salt Lake valley from 2240 to 2340 UTC 18 June ([Fig. 6b](#)). While flying at elevations of 1400–1700 m MSL (150–350 m AGL) in the south end of the valley the helicopter measured ozone concentrations near 60 ppb, which is consistent with values observed at the surface prior to the frontal passage at NAA, QHW, and MTMET ([Figs. 5c,d,e](#)). When the helicopter crossed the frontal boundary at 2313 UTC, ozone concentrations spiked to 115 ppb. As the helicopter traveled farther north, ozone concentrations were near 80 ppb, consistent with those observed at O3S02 and other fixed sites. The TRAX transect at this same time also confirms the higher ozone concentrations behind the lake-breeze front ([Fig. 6b](#)). The similarity of the ozone concentrations observed at the helicopter's flight level and those at the ground indicates strong vertical mixing below 1700 m MSL (300 m AGL). The ozone concentrations at the lake-breeze front in excess of 100 ppb measured by the high-frequency sampling undertaken on board the helicopter likely results from convergence of polluted air within the lake-breeze boundary layer.

b. WRF Model simulation of 17–18 June lake breezes

We briefly illustrate how inaccurate specification of the areal extent and temperature of the GSL affects HRRR model analyses and forecasts. [Figures 3a and 3b](#) show the HRRR 1-h forecasts and analyses of vertical profiles of temperature, moisture, and wind valid at 1200 UTC 18 June and 0000 UTC 19 June, respectively, at SLC. As a reminder, the HRRR-defined lake is larger and colder than that observed ([Fig. 2](#)). The largest deviations in the 1-h forecasts relative to those observed are evident in the afternoon, with lower temperatures and excessive low-level moisture forecasted in the boundary layer. This problem is exacerbated at longer lead times; for example, the HRRR 12-h forecast of surface potential temperature valid at this time is less than 312 K, leading to a cooler lake boundary layer than that observed (not shown). As should be expected, the vertical profiles from the HRRR analyses are constrained strongly by the observed sounding available at this location, leading, for example, to analyzed boundary layer winds at 0000 UTC from the north as an adjustment of the northeasterly 1-h forecast winds to the observed northwesterly winds. Vertical profiles from the WRF simulation are also shown in [Fig. 3](#). This simulation, with reduced lake size

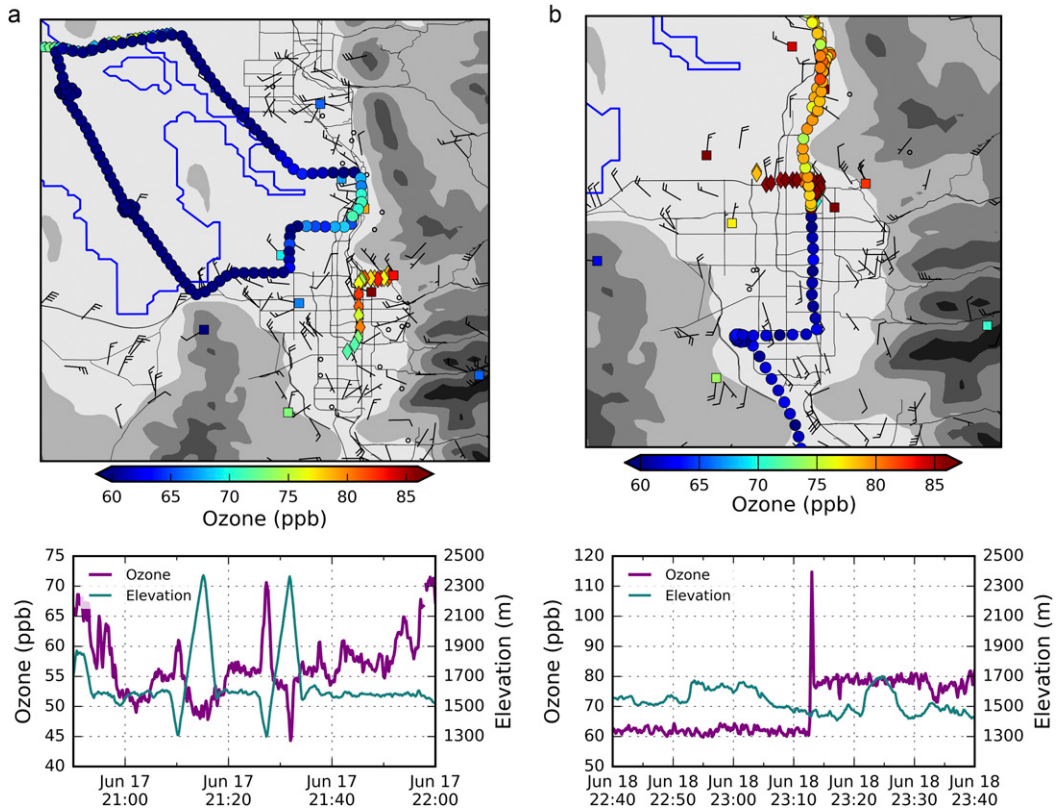


FIG. 6. Ozone observations according to color bar (top) between (a) 2050–2200 UTC 17 Jun and (b) 2240–2340 UTC 18 Jun 2015. Mobile ozone observations from the KSL-TV news helicopter (circles) and TRAX trains (diamonds) are plotted every 30 s and 3 min, respectively. Station sites show the most recent ozone (squares) and vector winds (barbs) observations within the hour ending at 2340 UTC. Major roads are drawn in black, with terrain shaded gray and the lake outlined in blue. (bottom) Time series of ozone concentration (purple) and elevation (teal) during the helicopter flights. As a reference, surface elevation is \sim 1300 m.

and higher temperature, increases the temperature and decreases the low-level moisture in the boundary layer at 0000 UTC relative to the HRRR 1-h forecasts.

Returning to Fig. 5, the passages of the simulated lake-breeze circulations at those locations are contrasted to those observed. While the simulated temperature at GSLBY is higher than that observed during both days (Fig. 5a), comparisons at other sites over the main body of the GSL suggest that the simulated lake boundary layer over the GSL remains too cool and shallow even after raising the lake surface temperature and allowing several days of model spinup for the boundary layer over the lake to adjust to that modified temperature. The penetration of the southerly flow associated with the land breezes at GSLBY is evident in both the observations and simulation during the early morning hours of both days followed by a flow reversal to northerly or northwesterly.

To the north of the SLC airport at O3S02 during both afternoons, the model tends to be too cold and develops northerly flow during the midday that misses the subtle westerly wind shifts that may have led to the noticeable

changes in ozone concentrations at this location (Fig. 5b). For example, the simulated lake breeze pushes cooler air from the northwest across O3S02 by 1700 UTC on 18 June, 3 h before it was observed to penetrate in the westerly burst mentioned previously (Figs. 4e and 5b).

In the northwestern sector of the valley at NAA (Fig. 5c), the simulated south-southeasterly oriented land breezes during both mornings at the surface are weaker and are followed by strong sustained northerly flows after 1700 UTC on 17 June and 1900 UTC on 18 June. Sharp, sustained temperature declines after the passage of the lake-breeze front in the simulation illustrate the stronger than observed intensity of the lake-breeze air mass. The termination of the lake breeze at NAA is also more distinct earlier with a sharp temperature increase at 0100 UTC [1900 mountain daylight time (MDT)] on both evenings.

The earlier timing and stronger intensity of the simulated lake-breeze frontal passages on 17 and 18 June are also apparent at QHW and MTMET (Figs. 5d,e). The sudden burst of southerly flow after 1700 UTC 18 June is

captured in the simulation but was shorter in duration than that observed. Hence, the lack of strong opposing flow in the simulation led to an earlier onset of the lake breeze down the valley.

Even after our adjustments to the areal extent and temperature of the GSL and urban canopy, our simulation has a stronger lake breeze at the surface that started down the Salt Lake valley earlier than observed, particularly on 18 June. However, the simulation provides a wealth of information on the evolution and structure of the lake breezes, as will be shown hereafter. We focus in the remainder of this section on the 18 June lake breeze that was observed to have higher ozone concentrations within it and lower concentrations in advance of it.

[Figure 7](#) delineates the progression of the observed, analyzed, and simulated surface lake-breeze front in the Salt Lake valley between 1800 and 2300 UTC (local 1200–1700 LT). Only simulated fields below 1500 m MSL are shown to emphasize the conditions within the lower parts of the valley. We review first the observed progression of the lake-breeze front (dashed lines in the center and right panels of [Fig. 7](#); see also [Fig. 4](#)). The leading edge of the lake breeze remains quasi-stationary from 1800 to 2000 UTC as a result of the aforementioned strong southerly opposing flow ([Figs. 7a–c](#)). Then, the southerly flow wanes, particularly in the central section of the valley; the front advances ([Fig. 7d](#)) and subsequently continues downvalley ([Figs. 7d,e](#)), reaching the southern extent at approximately 0220 UTC that evening (not shown).

Notice how the HRRR analyses handle the lake-breeze front shown in the left panels in [Fig. 7](#). The HRRR positions the front at 1800 UTC in the eastern half of the valley approximately 12 km farther south than was observed. During the rest of the afternoon, the HRRR lake-breeze front remains quasi-stationary near the northern extent of the valley with little change in its frontal position and orientation. The magnitude of the meridional winds on either side of the frontal zone between 1800 and 2000 UTC vary from hour to hour, perhaps because of differences in which data assets were assimilated by the HRRR. The HRRR analyses incorrectly locate the front at the north end of the valley with little to no upvalley progression during the afternoon. By the time the observed lake-breeze front reached the southern terminus of the valley, the HRRR analysis shows a weakening front still located north of the center of the valley an hour before the lake-breeze circulation collapses (not shown).

The center panels in [Fig. 7](#) show the near-surface moisture content and 10-m meridional wind with vector winds plotted every 3 km. The meridional wind component is a proxy for the TDWR radial velocities in [Fig. 4](#)

such that the simulated front is objectively identified as the location where the meridional wind component reverses and, hence, convergent frontogenesis is particularly evident. As should be expected, the model's inability to develop a sustained strong flow opposing the lake breeze leads to the front being too far south in the central portion of the valley in the early afternoon ([Figs. 7a,b](#)). Subsequently, after 1900 UTC ([Fig. 7c](#)), the front begins to move down the valley too early and too fast by about 3 km h^{-1} , causing it to reach the southern terminus of the valley several hours earlier than observed ([Fig. 7f](#)). However, the general features of the front's evolution are captured, with a low mixing ratio and southerly winds in advance of the front and a higher mixing ratio and northerly winds to its rear.

The right panels in [Fig. 7](#) show vertical velocity and vector winds on the seventh level of the terrain-following model coordinate, at approximately 1000 m AGL. Dashed and solid lines again represent the approximate frontal position at the surface. The near-surface convergent frontogenesis leads to upward motion at the frontal boundary coupled to descending motion in its wake that resembles the vertical motion patterns expected aloft that are often associated with a well-defined lake-breeze frontal head ([Zumpfe and Horel 2007; Crosman and Horel 2016](#)).

Time-height sections of potential temperature and meridional wind at NAA for the lake-breeze events on 17 and 18 June are shown in [Figs. 8a and 8b](#), respectively. The strong, shallow stable layers during the early morning hours mix out by 1600 UTC on both days but a warmer and deeper boundary layer through the lowest kilometer is evident on 18 June ([Fig. 8b](#)). One other difference between the two days is the timing of the frontal passage. On 17 June, the lake breeze transits NAA at 1700 UTC, while on 18 June the frontal passage is delayed by almost 2 h. This delay is caused by the increased strength of the opposing southerly meridional flow below 2300 m MSL on 18 June. With this increased convergent frontogenesis there is a well-defined frontal head on 18 June as it passes over NAA ([Fig. 8b](#)). A frontal head only develops on 17 June when the front reaches the southern terminus of the valley (not shown). On both days, northerly winds within the lake breeze continue until near sunset (0200 UTC), after which the lake breeze collapses.

The dynamic transport of pollutants by a strong lake-breeze front, using the 18 June case, is now illustrated. Potential temperature and vertical motion along the 3-km-wide A–B cross section ([Fig. 9a](#)) are shown for 1800, 1900, and 2000 UTC 18 June in [Figs. 9b–d](#), respectively. The well-mixed, warm boundary layer in the lowest kilometer in advance of the front is rapidly replaced

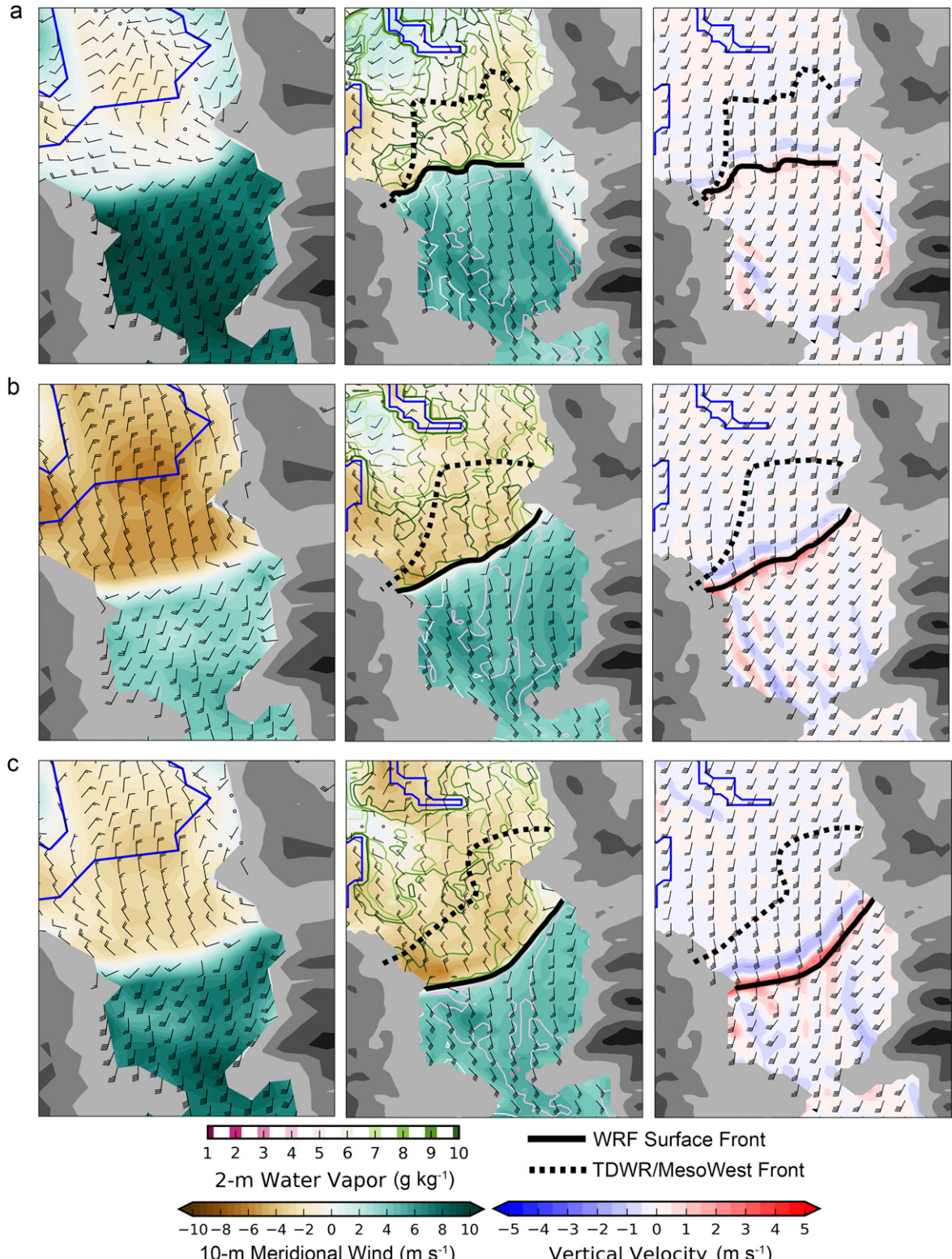


FIG. 7. Wind and moisture fields at (a) 1800, (b) 1900, (c) 2000 (d) 2100 (e) 2200, and (f) 2300 UTC 18 Jun 2015. Lake boundaries in HRRR and WRF are outlined in blue. For reference, the dashed and solid lines represent the progression of the observed and simulated lake-breeze fronts, respectively. (left) HRRR analysis 10-m meridional wind (shading) and 10-m vector winds (barbs). (center) WRF 10-m meridional wind (shading), 10-m vector winds (barbs), and 2-m water vapor mixing ratio (contours). (right) WRF Model level 7 (~1000 m AGL) vertical velocity (shading) and vector winds (barbs). Barbs are plotted every 3 km where half and full barbs and flags denote 1, 2, and 10 m s^{-1} , respectively.

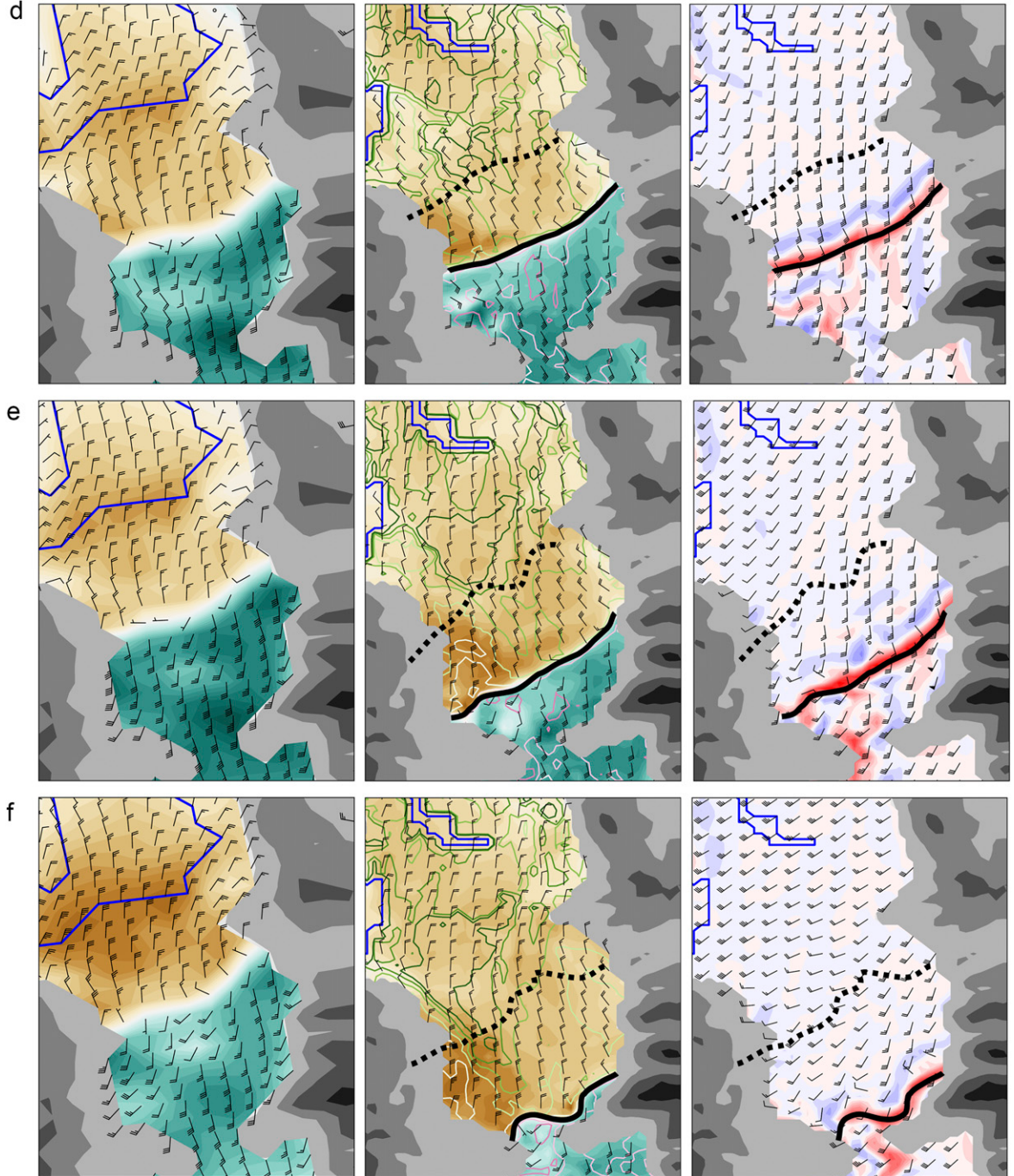


FIG. 7. (Continued)

as the front passes by with a cooler and shallower lake-breeze boundary layer. The strong rising–sinking couplets ($0.5\text{--}2.5 \text{ m s}^{-1}$) at the leading edge of the lake-breeze front head previously shown in Fig. 7 are well defined here as well.

Passive tracers emitted every time step are used to visualize the dispersion and transport of pollutants in the

Salt Lake valley as they interact with the lake-breeze front. The source regions of these tracers are two $5 \text{ km} \times 15 \text{ km}$ areas at the north and south ends of the Salt Lake valley, shown in Fig. 9a. At the beginning of each model time step, one tracer element is introduced at the lowest three model levels of each grid box in those source regions. This equates to 225 tracer particles released in each

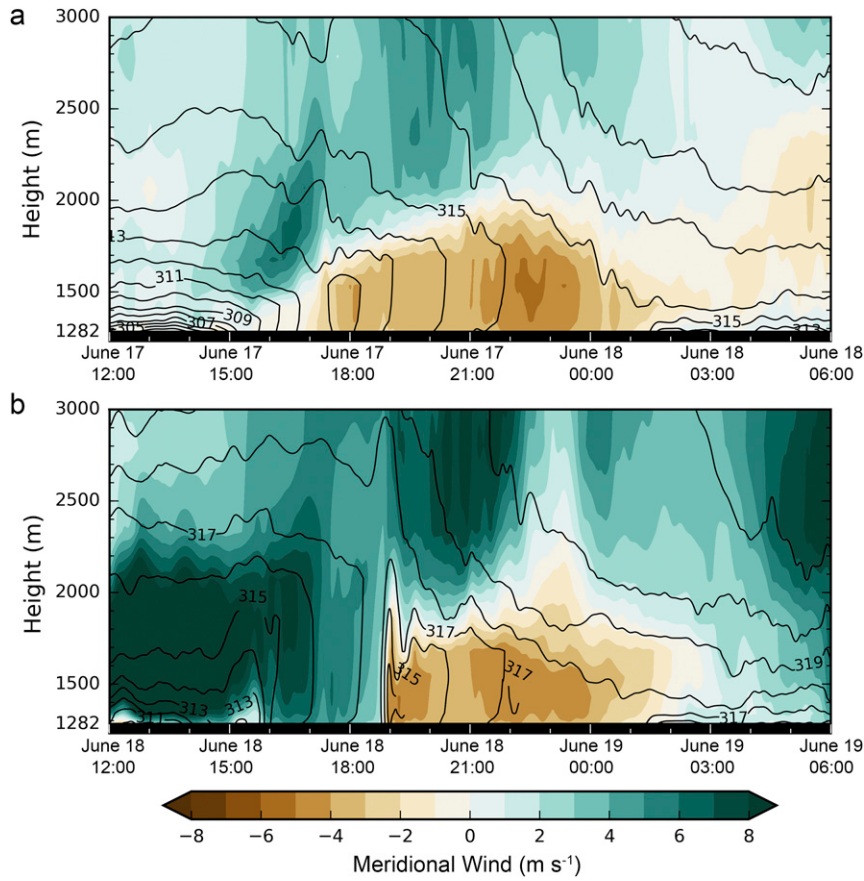


FIG. 8. Time–height section of simulated meridional wind (shading) and potential temperature (contours at 1-K intervals) at NAA (a) from 1200 UTC 17 Jun to 0600 UTC 18 Jun 2015 and (b) from 1200 UTC 18 Jun to 0600 UTC 19 Jun 2015.

of the two source regions every time step, which are then advected within the domain by the wind field. Particle counts along the 3-km-wide cross section (Fig. 9a) emitted between 1700 and 2000 UTC 18 June are shown at 1800, 1900, and 2000 UTC in Figs. 9b–d.

The blue tracers emitted at the south end of the valley illustrate how precursor pollutants and ozone in the deep boundary layer ahead of the front may be mixed vertically, advected northward, and lofted over the lake-breeze air. Plan-view maps of the tracer counts (not shown) indicate that those tracers are transported aloft northeastward across the Wasatch Mountains, which is consistent with the upper-level flows evident in Fig. 7. Red tracers from the north end of the Salt Lake valley illustrate the dispersion of pollutants within the lake breeze. These tracers are transported laterally up the valley and confined near the surface by the capping stable layer, except for the lofting of tracers within the head of the lake-breeze front where vertical motions are maximized. Turbulent mixing aloft likely dilutes the tracer concentrations from both source regions as

the lake-breeze front travels southward. Although the movement of the simulated lake-breeze front down the valley is too rapid, the behavior of the passive tracers illustrated in Fig. 9 is generally consistent with the observations by the fixed and mobile platforms. That is, blue tracers mixed within a deeper boundary layer are more diluted than red tracers, which are concentrated in a shallow layer within the lake breeze. A simulation using a coupled atmospheric-air chemistry model would likely improve our understanding of the high ozone concentration at the leading edge of the lake-breeze front.

4. Summary

The impact of lake breezes on summer ozone concentrations in the Salt Lake valley was investigated using data from GSLSO₃S conducted during summer 2015. Over the course of a few days in mid-June, ozone built up in the Salt Lake valley to unhealthy levels. The characteristics of the lake breeze on 17 June conformed to typical lake breezes previously studied in the Salt Lake

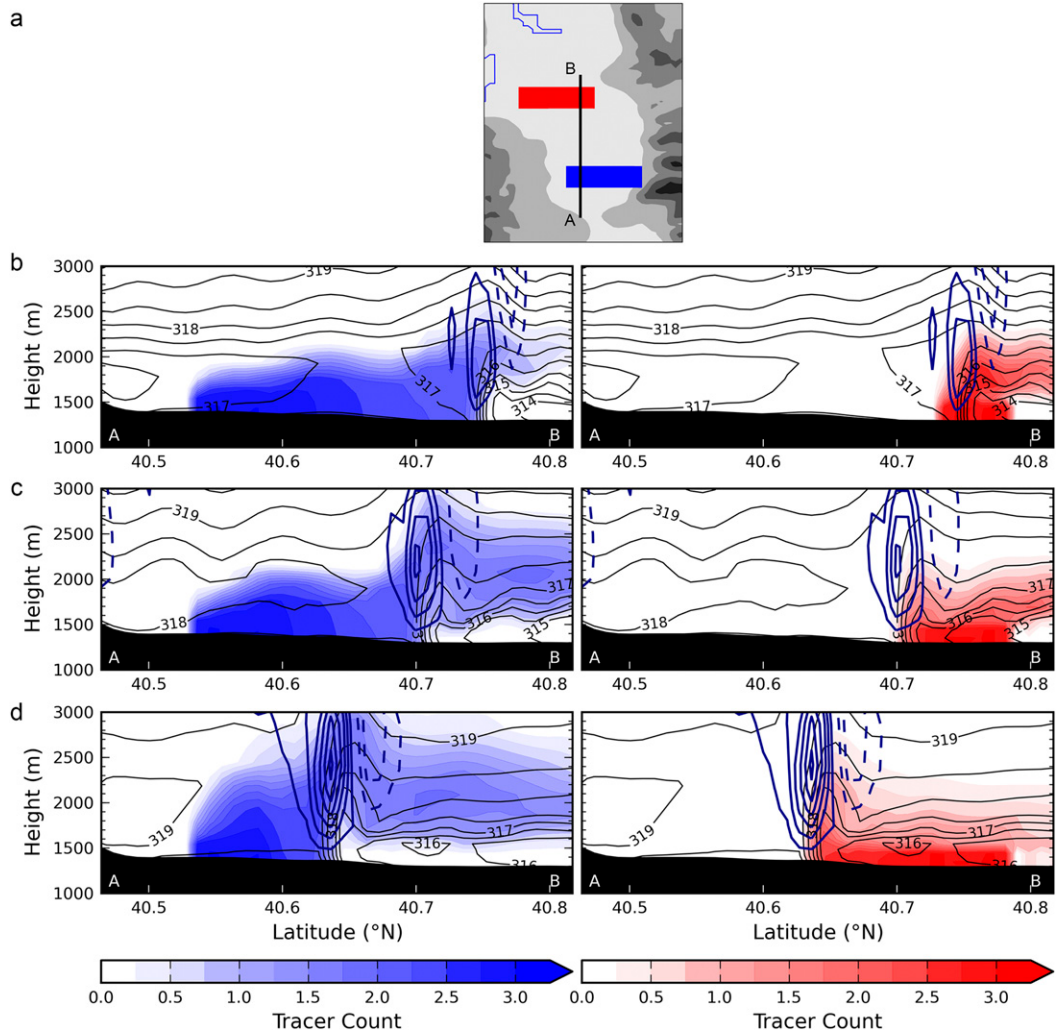


FIG. 9. (a) Cross-sectional orientation through the Salt Lake valley from A to B and locations of source regions of southern (blue) and northern (red) tracers. Potential temperature (black contours at 0.5-K intervals), upward (blue solid) and downward (blue dashed) vertical velocities (contoured at 0.5 m s^{-1}), and passive tracer concentrations at (b) 1800, (c) 1900, and (d) 2000 UTC 18 Jun 2015. Denoted is the transport of the (left) southern and (right) northern tracers. The cross section is 3 km wide, and the number of tracers has been summed and the potential temperature and vertical velocity averaged across its width.

valley, including distinct pulses up the valley in the afternoon until the northerly lake-breeze flow filled the entire valley by 0000 UTC. The highest midday ozone concentrations were found north of the Salt Lake valley at O3S02, referred to as Farmington Bay. That area is surrounded by a mix of permanent wetland and highly reflective playa with urban areas to its east and south. The availability of biogenic and anthropogenic emissions combined with enhanced photochemical production during the morning may help to explain the higher ozone concentrations at midday there. Based on an afternoon helicopter overflight on 17 June, ozone concentrations over the main body of the GSL to the northwest of the Salt Lake valley were lower than in the Farmington Bay area.

Hence, the lake breeze on 17 June tended to transport lower ozone concentrations toward the east and southeast behind the lake breeze.

On 18 June, opposing southerly winds kept the afternoon lake breeze at bay until 2100 UTC when a strong lake-breeze front pushed south through the Salt Lake valley, several hours later than the northerly lake-breeze pulses observed the previous afternoon. Robust horizontal and vertical mixing within the southerly flow ahead of the lake-breeze front likely contributed to ozone concentrations prior to the passage of the lake-breeze front that reflect the interplay between the advection of regional background ozone concentrations and photochemical production under way within the urban environment.

The shallow boundary layer within the lake breeze, combined with convergent frontogenesis at the leading edge of the lake-breeze front, led to the observed strong ozone gradient across the frontal boundary, that is, a sharp ~ 20 -ppb increase in ozone at surface stations as well as aloft between 1400 and 1700 m MSL (100–300 m AGL). After the lake-breeze front passed, ozone levels remained higher than they were the previous day, contributing to the 8-h ozone standard being exceeded at many locations within the valley. The causes for the high ozone concentrations behind the front are difficult to ascertain on the basis of the observations available at that time. We speculate that the following factors were likely contributing: clear skies on 17 June and after sunrise on 18 June, facilitating continued ozone production offshore and over the wetlands and playa surfaces to the north of the valley; additional nocturnal transport of precursor chemicals away from the urban areas and reduced ozone deposition over the lake; and decreased vertical mixing within the lake-breeze's stable boundary layer. Further research will be necessary to determine the relative importance of these factors.

While the 3-km resolution HRRR analyses during this 2-day period help to resolve many aspects of the complex thermal and terrain flows in northern Utah, subtle meteorological features such as the intensity of the southerly flow during the late morning on 18 June were not captured by them. Overly intense afternoon lake breezes predicted by the HRRR may result in part from imperfect specification of the areal extent and temperature of the GSL. Our research simulation encompassing this 2-day period utilizing corrections to the lake size and temperature did not deepen the lake boundary layer or weaken the simulated lake breeze as much as we were expecting. We suspect one reason for the shallow boundary layer is the overly cool and large lake in the HRRR analyses used to initialize the model. Additional model improvements to this and other lake breezes might be achieved by increasing the spinup time to allow the modeled boundary layer to adjust to the modified surface state.

Another source of model error may be introduced by the Mellor–Yamada–Janjić planetary boundary layer parameterization used in this study (Table 1). Hu et al. (2010) found that the Mellor–Yamada–Janjić scheme had larger temperature, moisture, and boundary layer height biases than other boundary layer schemes for the Galveston Bay area in Texas. We intend to examine other boundary layer parameterizations including the Mellor–Yamada–Nakanishi–Niino parameterization that has been shown to simulate marine boundary layers with greater fidelity (Coniglio et al. 2013; Banks et al. 2016).

While far from perfect, our model simulation at 1-km grid spacing captured many of the features of the weaker

lake breeze on 17 June and the stronger lake breeze on 18 June. However, it missed the subtle, short-lived strengthening of the southerly opposing flow on 18 June that affected the timing of the lake-breeze propagation. Passive tracers released within the model simulation on 18 June highlight the distinctly different transport ahead and behind of this strong lake-breeze front.

The findings presented in this work should be useful to local air quality forecasters and modelers in other coastal regions where lake- or sea-breeze circulations affect pollution levels. This study highlights how the timing and intensity of subtle mesoscale features, such as the short-duration burst of southerly flow observed midday on 18 June, can affect a lake breeze and ozone concentrations within an urban region in the afternoon.

Acknowledgments. We appreciate the assistance of everyone involved in the GSLSO₃S, including those at the Utah Division of Air Quality (Seth Arens, Munkh Baassandorj, Katherine Chapman, and Mark Squire), the University of Utah (Alex Jacques, Ansley Long, Luke Leclair-Marzolf, Will Howard, Jeff Jenkins, Allyson Dugan, Sebastian Hoch, Susan Bush, Xia Dong, Nola Lucke, Taylor McCorkle, Dillon Ulrich, Tom Gowan, Chris Galli, and Fahad Alotaibi), Weber State University (John Sohl, Sheri Trbovich, Jeff Page, Lisa Finlinson, Elizabeth Dowell, William Dowell, Murielle Shallbetter, and Nicholas Allen), and Randy Martin at Utah State University. We also appreciate the help provided by KSL-TV news helicopter pilot Ben Tidswell and the staff of the Utah Transit Authority, particularly Teresa Jessen. We also acknowledge Cory Angeroth and Ryan Rowland from the U.S. Geological Survey for the Great Salt Lake buoy data. The support and resources from the Center for High Performance Computing at the University of Utah are gratefully acknowledged. This research was supported by grants from the Utah Division of Air Quality and the National Science Foundation (Grant ACI 1443046).

REFERENCES

- Angevine, W. M., M. Tjernström, and M. Žagar, 2006: Modeling of the coastal boundary layer and pollutant transport in New England. *J. Appl. Meteor. Climatol.*, **45**, 137–154, doi:[10.1175/JAM2333.1](https://doi.org/10.1175/JAM2333.1).
- , L. Eddington, K. Durkee, C. Fairall, L. Bianco, and J. Brioude, 2012: Meteorological model evaluation for CalNex 2010. *Mon. Wea. Rev.*, **140**, 3885–3906, doi:[10.1175/MWR-D-12-00042.1](https://doi.org/10.1175/MWR-D-12-00042.1).
- Arritt, R. W., 1989: Numerical modelling of the offshore extent of sea breezes. *Quart. J. Roy. Meteor. Soc.*, **115**, 547–570, doi:[10.1002/qj.49711548707](https://doi.org/10.1002/qj.49711548707).
- , 1993: Effects of the large-scale flow on characteristic features of the sea breeze. *J. Appl. Meteor. Climatol.*, **32**, 116–125, doi:[10.1175/1520-0450\(1993\)032<0116:EOTLSF>2.0.CO;2](https://doi.org/10.1175/1520-0450(1993)032<0116:EOTLSF>2.0.CO;2).

- Banks, R. F., J. Tirana-Alsina, J. M. Baldasano, F. Rocadenbosch, A. Papayannis, S. Solomos, and C. G. Tzanis, 2016: Sensitivity of boundary-layer variables to PBL schemes in the WRF model based on surface meteorological observations, lidar, and radiosondes during the HygraA-CD campaign. *Atmos. Res.*, **176–177**, 185–201, doi:10.1016/j.atmosres.2016.02.024.
- Banta, R. M., and Coauthors, 2005: A bad air day in Houston. *Bull. Amer. Meteor. Soc.*, **86**, 657–669, doi:10.1175/BAMS-86-5-657.
- Bao, J.-W., S. A. Michelson, P. O. G. Persson, I. V. Djalalova, and J. M. Wilczak, 2008: Observed and WRF-simulated low-level winds in a high-ozone episode during the Central California Ozone Study. *J. Appl. Meteor. Climatol.*, **47**, 2372–2394, doi:10.1175/2008JAMC1822.1.
- Benjamin, S. G., and Coauthors, 2016: A North American hourly assimilation and model forecast cycle: The Rapid Refresh. *Mon. Wea. Rev.*, **144**, 1669–1694, doi:10.1175/MWR-D-15-0242.1.
- Burley, J. D., S. Theiss, A. Bytnerowicz, A. Gertler, S. Schilling, and B. Zielinska, 2015: Surface ozone in the Lake Tahoe basin. *Atmos. Environ.*, **109**, 351–369, doi:10.1016/j.atmosenv.2015.02.001.
- Coniglio, M. C., J. Correia, P. T. Marsh, and F. Kong, 2013: Verification of convection-allowing WRF model forecasts of the planetary boundary layer using sounding observations. *Wea. Forecasting*, **28**, 842–862, doi:10.1175/WAF-D-12-00103.1.
- Crosman, E., and J. Horel, 2009: MODIS-derived surface temperature of the Great Salt Lake. *Remote Sens. Environ.*, **113**, 73–81, doi:10.1016/j.rse.2008.08.013.
- , and —, 2010: Sea and lake breezes: A review of numerical studies. *Bound.-Layer Meteor.*, **137**, 1–29, doi:10.1007/s10546-010-9517-9.
- , and —, 2012: Idealized large-eddy simulations of sea and lake breezes: Sensitivity to lake diameter, heat flux and stability. *Bound.-Layer Meteor.*, **144**, 309–328, doi:10.1007/s10546-012-9721-x.
- , and —, 2016: Winter lake breezes near the Great Salt Lake. *Bound.-Layer Meteor.*, **159**, 439–464, doi:10.1007/s10546-015-0117-6.
- EPA, 2015: Implementation of the 2015 primary ozone NAAQS: Issues associated with background ozone. Environmental Protection Agency White Paper for Discussion, 27 pp. [Available online at <https://www.epa.gov/sites/production/files/2016-03/documents/whitepaper-bgo3-final.pdf>.]
- Foley, T., E. A. Betterton, R. Jacko, and J. Hillery, 2011: Lake Michigan air quality: The 1994–2003 LADCO Aircraft Project (LAP). *Atmos. Environ.*, **45**, 3192–3202, doi:10.1016/j.atmosenv.2011.02.033.
- Gaza, R., 1998: Mesoscale meteorology and high ozone in the northeast United States. *J. Appl. Meteor. Climatol.*, **37**, 961–977, doi:10.1175/1520-0450(1998)037<0961:MMAHOI>2.0.CO;2.
- Gilliam, R. C., S. Raman, and D. D. S. Niyogi, 2004: Observational and numerical study on the influence of large-scale flow direction and coastline shape on sea-breeze evolution. *Bound.-Layer Meteor.*, **111**, 275–300, doi:10.1023/B:BOUN.0000016494.99539.5a.
- Goldberg, D. L., C. P. Loughner, M. Tzortziou, J. W. Stehr, K. E. Pickering, L. T. Marufu, and R. R. Dickerson, 2014: Higher surface ozone concentrations over the Chesapeake Bay than over the adjacent land: Observations and models from the DISCOVER-AQ and CBODAQ campaigns. *Atmos. Environ.*, **84**, 9–19, doi:10.1016/j.atmosenv.2013.11.008.
- Hastie, D. R., and Coauthors, 1999: Observational evidence for the impact of the lake breeze circulation on ozone concentrations in southern Ontario. *Atmos. Environ.*, **33**, 323–335, doi:10.1016/S1352-2310(98)00199-X.
- Hayden, K. L., and Coauthors, 2011: Aircraft study of the impact of lake-breeze circulations on trace gases and particles during BAQS-Met 2007. *Atmos. Chem. Phys.*, **11**, 10 173–10 192, doi:10.5194/acp-11-10173-2011.
- Horel, J., and Coauthors, 2002: MesoWest: Cooperative mesonets in the western United States. *Bull. Amer. Meteor. Soc.*, **83**, 211–225, doi:10.1175/1520-0477(2002)083<0211:MCMITW>2.3.CO;2.
- , E. Crosman, A. Jacques, B. Blaylock, S. Arens, A. Long, J. Sohl, and R. Martin, 2016: Summer ozone concentrations in the vicinity of the Great Salt Lake. *Atmos. Sci. Lett.*, **17**, 480–486, doi:10.1002/asl.680.
- Hu, X.-M., J. W. Neilson-Gammon, and F. Zhang, 2010: Evaluation of three planetary boundary layer schemes in the WRF model. *J. Appl. Meteor. Climatol.*, **49**, 1831–1844, doi:10.1175/2010JAMC2432.1.
- Hwang, M.-K., Y.-K. Kim, S. N. Oh, H. W. Lee, and C.-H. Kim, 2007: Identification and interpretation of representative ozone distributions in association with the sea breeze from different synoptic winds over the coastal urban area in Korea. *J. Air Waste Manage. Assoc.*, **57**, 1480–1488, doi:10.3155/1047-3289.57.12.1480.
- Jaffe, D., 2011: Relationship between surface and free tropospheric ozone in the western U.S. *Environ. Sci. Technol.*, **45**, 432–438, doi:10.1021/es1028102.
- Ji, H.-E., S.-H. Lee, and H.-W. Lee, 2013: Characteristics of sea breeze front development with various synoptic conditions and its impact on lower troposphere ozone formation. *Adv. Atmos. Sci.*, **30**, 1461–1478, doi:10.1007/s00376-013-2256-3.
- Lareau, N. P., and J. Horel, 2015: Dynamically induced displacements of a persistent cold-air pool. *Bound.-Layer Meteor.*, **154**, 291–316, doi:10.1007/s10546-014-9968-5.
- Lennartson, G. J., and M. D. Schwartz, 2002: The lake breeze-ground-level ozone connection in eastern Wisconsin: A climatological perspective. *Int. J. Climatol.*, **22**, 1347–1364, doi:10.1002/joc.802.
- Levy, I., and Coauthors, 2010: Unraveling the complex local-scale flows influencing ozone patters in the southern Great Lakes of North America. *Atmos. Chem. Phys.*, **10**, 10 895–10 915, doi:10.5194/acp-10-10895-2010.
- Lombardo, K., E. Sinsky, Y. Jia, M. M. Whitney, and J. Edson, 2016: Sensitivity of simulated sea breezes to initial conditions in complex coastal regions. *Mon. Wea. Rev.*, **144**, 1299–1320, doi:10.1175/MWR-D-15-0306.1.
- Lu, R., and R. P. Turco, 1995: Air pollutant transport in a coastal environment—II. Three-dimensional simulations over Los Angeles basin. *Atmos. Environ.*, **29**, 1499–1518, doi:10.1016/1352-2310(95)00015-Q.
- Ludwig, F. L., J. Horel, and C. D. Whiteman, 2004: Using EOF analysis to identify important surface wind patterns in mountain valleys. *J. Appl. Meteor.*, **43**, 969–983, doi:10.1175/1520-0450(2004)043<0969:UEATII>2.0.CO;2.
- Monks, P. S., and Coauthors, 2015: Tropospheric ozone and its precursors from the urban to the global scale from air quality to short-lived climate forcer. *Atmos. Chem. Phys.*, **15**, 8889–8973, doi:10.5194/acp-15-8889-2015.
- Oh, I.-B., Y.-K. Kim, H. W. Lee, and C.-H. Kim, 2006: An observational and numerical study on the effects of the late sea breeze on ozone distributions in the Busan metropolitan area, Korea. *Atmos. Environ.*, **40**, 1284–1298, doi:10.1016/j.atmosenv.2005.10.049.
- Porson, A., D. G. Steyn, and G. Schayes, 2007: Sea breeze scaling from numerical model simulations, part II: Interactions

- between the sea breeze and slope flows. *Bound.-Layer Meteor.*, **122**, 31–41, doi:[10.1007/s10546-006-9092-2](https://doi.org/10.1007/s10546-006-9092-2).
- Sills, D. M. L., J. R. Brook, I. Levy, P. A. Makar, J. Zhang, and P. A. Taylor, 2011: Lake breezes in the southern Great Lakes region and their influence during BAQS-Met 2007. *Atmos. Chem. Phys.*, **11**, 7955–7973, doi:[10.5194/acp-11-7955-2011](https://doi.org/10.5194/acp-11-7955-2011).
- Sousa, S. I. V., M. C. M. Alvim-Ferraz, and F. G. Marins, 2013: Health effects of ozone focusing on childhood asthma: What is now known—A review from an epidemiological point of view. *Chemosphere*, **90**, 2051–2058, doi:[10.1016/j.chemosphere.2012.10.063](https://doi.org/10.1016/j.chemosphere.2012.10.063).
- Stauffer, R. M., and Coauthors, 2015: Bay breeze influence on surface ozone at Edgewood, MD during July 2011. *J. Atmos. Chem.*, **72**, 335–353, doi:[10.1007/s10874-012-9241-6](https://doi.org/10.1007/s10874-012-9241-6).
- Stewart, J. Q., C. D. Whiteman, W. J. Steenburgh, and X. Bian, 2002: A climatological study of thermally driven wind systems of the U.S. Intermountain West. *Bull. Amer. Meteor. Soc.*, **83**, 699–708, doi:[10.1175/1520-0477\(2002\)083<0699:ACSOTD>2.3.CO;2](https://doi.org/10.1175/1520-0477(2002)083<0699:ACSOTD>2.3.CO;2).
- Talbot, R., H. Mao, and B. Sive, 2005: Diurnal characteristics of surface level O₃ and other important trace gases in New England. *J. Geophys. Res.*, **110**, D09307, doi:[10.1029/2004JD005449](https://doi.org/10.1029/2004JD005449).
- Wentworth, G. R., J. G. Murphy, and D. M. L. Sills, 2015: Impact of lake breezes on ozone and nitrogen oxides in the greater Toronto area. *Atmos. Environ.*, **109**, 52–60, doi:[10.1016/j.atmosenv.2015.03.002](https://doi.org/10.1016/j.atmosenv.2015.03.002).
- Wurtsbaugh, W., C. Miller, S. Null, P. Wilcock, M. Hahnberger, and F. Howe, 2016: Impacts of water development on Great Salt Lake and the Wasatch Front. Watershed Sciences Faculty Publications, Paper 875, 9 pp. [Available online at http://digitalcommons.usu.edu/wats_facpub/875.]
- Zumpfe, D. E., and J. Horel, 2007: Lake-breeze fronts in the Salt Lake valley. *J. Appl. Meteor. Climatol.*, **46**, 196–211, doi:[10.1175/JAM2449.1](https://doi.org/10.1175/JAM2449.1).